doi:10.1017/S1431927612003340
Microsc. Microanal. 18 (Suppl 2), 2012

Imaging 'Invisible' Dopant Atoms in Semiconductor Nanocrystals

A. A. Gunawan[1], A. Wills[1], M.G., Thomas[2], D. J. Norris[3], K. A. Mkhoyan[1]

[1]Chemical Engineering and Materials Science, University of Minnesota, Minneapolis, MN 55455
[2]Applied and Engineering Physics, Cornell University, Ithaca, NY 4853
[3]Department of Mechanical and Process Engineering ETH Zürich, 8006 Zürich, Switzerland

Incorporation of impurities, or dopant atoms, into semiconducting materials is a critical part in optimizing the performance of electronic devices. In nanoscale semiconductors such as nanocrystals (NCs), statistical fluctuations in the number and position of the dopant atoms can have a dramatic effect on the electronic and optical properties of the NCs. Hence, it is important to locate the position of dopant atoms. Annular dark-field scanning transmission electron microscopy is a powerful technique for such purpose, as demonstrated previously on various combinations of dopant atoms and host materials [1, 2]. However, those experiments require that the difference in atomic numbers between the host crystals and dopant atoms (ΔZ) be sufficiently large to yield a visible contrast in the image.

In this study, we utilized a spectrum imaging technique to simultaneously record electron energy loss spectra (EELS) and annular dark field – scanning transmission electron microscopy (ADF-STEM) images in order to identify Mn dopant atoms inside ZnSe NCs [3]. This enables dopant detection to be performed on a system of host crystals and dopant atoms which does not have a large ΔZ. This technique can be an alternative method in identifying dopant atoms inside materials whereby conventional ADF-STEM imaging is difficult to perform due to low ΔZ.

The ZnSe NCs were synthesized using high temperature organometallic solution based route [4]. The Mn doping was achieved by injecting dimethylmanganese into a mixture containing diethylzinc and Se. The number of incorporated Mn atoms can be tuned by varying the concentration of dimethylmanganese. Three types of samples were examined: (1) 2.9 nm diameter NCs with an average of 0.7 incorporated Mn atom per NC (singly doped), (2) 3.7 nm NCs with an average of 6.2 Mn atoms per NC (highly doped), and (3) 2 nm undoped NCs used for reference.

The spectrum imaging was performed using Nion aberration corrected Ultra-STEM at Cornell University. The accelerating voltage (100 kV) and beam current (~150 pA) were adjusted to minimize beam damage on the samples while still maintain a large signal to noise ratio. The resulting spectra were stored in 3-D matrices corresponding to the spatial (x, y) and energy loss data (z) and were filtered to remove counting noise. Mn $L_{2,3}$-edge spectrum from bulk Mn samples were used to perform a linear-least-square (LLS) fitting for each of the Mn $L_{2,3}$-edge signals from the NCs. A two-dimensional EELS map ($M(i,j)$) was then obtained following a relation $M(i,j) = G(i,j)S(i,j)$ where G and S represent the goodness of fit and intensity scaling factor respectively. The presence of Mn dopant atoms corresponding to a pixel is characterized by large values of G and S in $M(i,j)$ which was spatially correlated with the ADF-STEM image through the overlay process shown in Fig. 1a. This overlaid image is used to locate the presence of Mn dopant atoms in the NCs. In the case of highly doped NCs (sample 2) consistent detection of Mn is obtained as shown in Fig. 1b.

The local beam intensity of the STEM probe was calculated using Multislice simulations in order to estimate the expected EELS signals from the Mn atoms [5]. Fig. 2a shows intensity of the electron beam as it propagates through the NCs. The arrangement of atoms in each direction results in the strongest beam intensity along the [111] direction. The simulated *M(i,j)* for a 4 nm [111] ZnSe NC is shown in Fig. 2c whereby two Mn atoms are located 1.3 and 2.9 nm below the top surface. The simulation confirms the detectability of both Mn atoms with the stronger signal arises from the 1.3 nm deep Mn corresponding to the peak in the simulated beam intensity. These Mn atoms, however, are undetectable using sole ADF-STEM imaging (Fig. 2b) as the intensities of the doped column (circled) are indistinguishable from the adjacent columns.

References:

[1] P. M. Voyles et al., *Nature,* 416 (2002) 826.
[2] A. Mittal, K. A. Mkhoyan, *Ultramicroscopy* 111 (2011) 1101.
[3] A. A. Gunawan et al., *Nano Letters,* 11 (2011) 5553.
[4] D. J. Norris et al., *Nano Letters.,* 1 (2001) 3.
[5] E. J. Kirkland, *Advanced Computing in Electron Microscopy*, 2nd edition, Springer (2010).

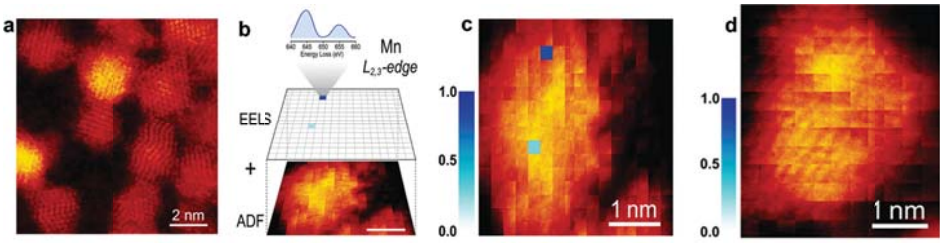

Fig. 1. (a). ADF-STEM image of Mn-doped ZnSe NCs (sample 1). (b) The extracted core-level EELS map for the Mn $L_{2,3}$-edge along with the corresponding ADF-STEM image of a Mn-doped ZnSe NCs (sample 2). (c) Overlap of the Mn $L_{2,3}$-edge intensity map and the ADF-STEM image for (b) Mn-doped ZnSe NCs (both shown in (b)) and (d) undoped ZnSe NCs (sample 3) showing no Mn EELS signals, as expected.

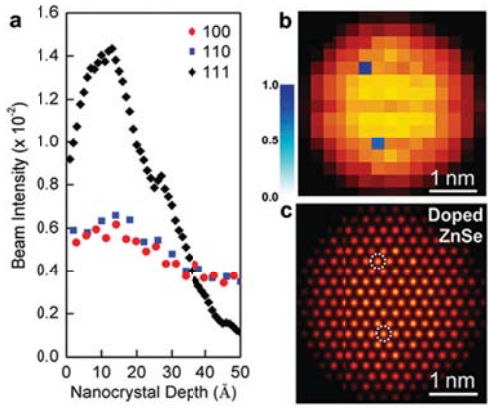

Fig. 2. (a) Calculated STEM electron beam intensity at the atomic column as it propagates along the [100], [110], and [111] directions in ZnSe NCs. (b) Simulated high resolution ADF-STEM image of a 4 nm ZnSe NC with two Mn dopants (circled) located 1.3 and 2.9 nm below the top surface. (c) Overlap of the simulated normalized Mn $L_{2,3}$-edge intensity map with the ADF-STEM image for the case in (b) under the experimental conditions used in Fig. 1b.